Cement and Concrete Research 39 (2009) 195–205

Contents lists available at ScienceDirect

Cement and Concrete Research

journal homepage: http://ees.elsevier.com/CEMCON/default.asp

Effect of heat-treatment and hydrostatic loading upon the poro-elastic properties of a mortar

Xiao-Ting Chen [a], C.A. Davy [a,*], F. Skoczylas [a], J.F. Shao [b]

[a] Laboratoire de Mécanique de Lille (LML), Ecole Centrale de Lille, BP 48, F-59651 Villeneuve d'Ascq Cedex, France
[b] Laboratoire de Mécanique de Lille (LML), and Polytech'Lille, Avenue Paul Langevin, F-59655 Villeneuve d'Ascq Cedex, France

ARTICLE INFO

Article history:
Received 3 March 2008
Accepted 5 December 2008

Keywords:
Mortar
Poro-elasticity
Thermal treatment
Hydrostatic stress
Micro-cracking

ABSTRACT

This contribution aims at identifying experimentally the poro-elastic properties of a cement-based material under different levels of confining pressure, and after a heat-treatment up to 400 °C. The model material used is a normalized mortar, with a (W/C) ratio of 0.5. After a given heating/cooling cycle, drained bulk modulus K_b, solid matrix bulk modulus K_s and Biot's coefficient b are measured at different confining pressure levels (with a maximum of 25 MPa).

Results show that under drained conditions, mortar stress–strain relationship evolves with increasing heat-treatment temperature from linear elastic with brittle failure (up to 105 °C heat treatment) to plastic and ductile (from 200 °C and above). Plastification testifies of material degradation under gradual confining pressure. At the microstructure scale, this is attributed to thermal damage after heat treatment above 105 °C, which consists mainly in various micro-cracking. This leads to easier failure of solid skeleton bridges (or trabecules), and to pore network collapse. Concomitantly to this, at given confining pressure P_c, secant drained bulk modulus K_b decreases monotonously, for heat-treatment temperatures above 105 °C. On the opposite, at given heat-treatment temperature above 105 °C, secant drained bulk modulus K_b increases when confining pressure is increased. This testifies of a solid matrix rigidification in the elastic domain, and it is attributed to increased skeleton compactness linked with pore network collapse. This is directly attributable to heat treatment followed by confinement.

At given confining pressure P_c, matrix bulk modulus K_s and Biot's coefficient b increase with heat-treatment temperature above 105 °C. The increase in b means that mortar becomes less and less cohesive and more and more of a granular nature. Moreover, Biot's coefficient b and solid matrix bulk modulus K_s are independent of confining pressure P_c for intact mortar, whereas they decrease for heat-treated mortars when P_c increases. From literature analysis alone, it was quite unexpected that after heat treatment, K_s should vary under confinement. This is interpreted as the closure, under confining pressure, of micro-void connections and of micro-cracks created by heat-treatment. Therefore, increasing confinement induces more and more occluded pores in the solid matrix, whereby K_s diminishes.

1. Introduction

This experimental study is the first part of a research program investigating the effects of temperature (up to 400 °C) and mechanical loading upon cement-based materials damage, poro-mechanical behaviour and transport properties. Indeed, cement-based materials are widely used in the civil engineering area where they may be subjected to both mechanical loading and relatively high temperatures, such as during fire accidents of tunnels or buildings, or in the context of radioactive waste storage. Exposure to high temperatures brings varied changes to cement-based materials properties, e.g. changes in their pore microstructure [1], hydraulic and mechanical properties [2–8], and their micro-cracking is also widely reported [9,10]. Yet, changes in their poro-mechanical properties have been scarcely identified experimentally, except, to our knowledge, in [11,12].

Nowadays, the Theory of Porous Media (TPM) [13–15] has proven useful to predict mechanical and hydraulic couplings between the porous skeleton and the pore fluids of various rocks, soils and even bone [16,17]. Indeed, the behaviour of these materials is notably influenced by the porous network size distribution, by the nature and amount of fluid present inside the porous network, all of which the TPM accounts for. It is also a useful tool for describing and explaining the evolutions and degradations of porous materials at the microstructure scale (i.e. changes in morphology) or at the macroscopic scale of a structure. For instance, experimental identification of the poro-mechanical properties of rocks is widely available in the literature [18–24]. In particular, for a homogeneous mono-mineral Bourgogne limestone, M. Lion et al. [23] have validated a linear and isotropic poroelasticity model, and identified

* Corresponding author. Tel.: +33 3 20 67 60 84; fax: +33 3 20 33 53 52.
E-mail address: catherine.davy@ec-lille.fr (C.A. Davy).

0008-8846/$ – see front matter © 2008 Elsevier Ltd. All rights reserved.
doi:10.1016/j.cemconres.2008.12.001

a whole set of poro-elastic parameters. A second contribution by M. Lion et al. [24] has aimed at identifying the effect of heating up to 250 °C upon those poro-elastic properties. All tests have been performed using ethanol as a neutral saturating fluid and residual values (after heating/cooling) are identified for K_b, K_u, K_s, b, B and M. Except for Biot's coefficient b, all parameters have been shown to decrease with thermal treatment up to 250 °C, the higher decrease corresponding to undrained parameters K_u, B and M. Contrarily to intact limestone, heat-treated limestone displays slight micro-crack closure under confinement. This has been recorded at the beginning of drained hydrostatic tests (for confining pressures P_c up to about 15 MPa), and it is followed by a linear evolution of volumetric strain ε_v for higher P_c. While drained bulk modulus K_b decreases by 4% of its initial value only, the solid matrix bulk modulus K_s of Bourgogne limestone has been found to decrease by 14% of its initial value after a 250 °C heating/cooling cycle. This has been interpreted as a consequence of intra matrix micro-cracking created at temperatures above 150 °C, although micro-cracks have not been observed during subsequent SEM analysis at the micrometric scale. On the opposite, M. Sibai et al. [22] have shown that K_s may be considered constant for a Fontainebleau sandstone, even after a heating/cooling cycle of up to 800 °C. Changes in K_b for heating cycles up to 800 °C do not appear significant either, when recorded after the initial non linear phase (i.e. that due to crack closure under confinement) such as in [23,24].

Yet, for cement-based materials [25], a controversy has long existed as to whether the TPM is adequate due to the presence of non negligible amounts of structural water (inside nano- and micro-pores) as well as bulk water (inside macro-pores). Ulm et al. [25], Coussy [14] and Dormieux et al. [26] have proposed strong arguments in favour of the TPM for cement-based materials, and our contribution provides additional experimental arguments. In particular, Ulm et al. [25] decompose cement-based materials microstructure into four elementary levels (from '0' to 'III') with increasing scale, which allows further poro-mechanical modelling using continuum micro-mechanics tools. Contrarily to the well-known Feldman-Sereda layered model of the C–S–H [27], and following works by Jennings et al. [28,29], the nano-metric (10^{-9} to 10^{-10} m) level '0' is represented as the colloidal assembly of C–S–H globules with an inter globules gel porosity, either at a low density (LD) or at a higher density (HD). This level is supposed the largest scale at which the material properties are constant whatever the cement-based material considered, which justifies a continuum micro-mechanical approach. Micrometric scale level 'I' (below 10^{-6} m) is that of the C–S–H matrix, composed of the two different LD and HD C–S–H solid phases, in varying proportions, plus gel porosity: it is the largest scale currently accessible to mechanical testing (by nano-indentation [30]). Sub-millimetric level 'II' (below 10^{-4} m) includes the C–S–H matrix, non hydrated clinker phases, Portlandite crystals and macro-pores, while the macroscopic scale level 'III' is that of the mortar or concrete, and is composed of the cement paste plus sand (or aggregates). For a W/C=0.5 mortar made with a CEM I cement and a sand volume fraction of 1/3, with an assumption of b equal to 0.61 (HD C–S–H) or 0.71 (LD C–S–H), and K_s= 31.8 GPa at level '0', b (resp. K_b) is evaluated at 0.69 (resp. 15 GPa) at level 'I', while it decreases down to 0.54 (resp. increases up to 18.8 GPa) at the mortar macroscopic level 'III' scale. Yet, H.M. Jennings [31] has recently proposed a more accurate model for the C–S–H phase than that of the "globules" [28,29], that integrates the well-known Feldman-Sereda layered model. Using these developments, Dormieux et al. [26] have integrated various experimental data, and validated a micro-poro-mechanical model for the hydrating cement paste down to very low hydration degrees (of about 20%). At the microscopic scale, the hydrating paste is represented by a number of grains made of an anhydrous clinker core, surrounded by an "inner" HD C–S–H layer. These grains are surrounded by a matrix (also called "porous foam") composed of "outer" LD C–S–H and capillary pores, which respective proportions vary with increasing hydration. All C–S–H are assumed as the assembly of elementary layered bricks of a flattened shape (with structural gel porosity), such as in the Feldman-Sereda model [27] integrated by Jennings [31]. Poro-elastic coefficients may be derived from this modelling.

For a model (W/C)=0.5 mortar subjected to drying, Skoczylas et al. [12] have shown that poromechanical coupling has only a partial contribution to the decrease in elastic properties and to the increase in compressive strength. The latter is rather attributed to local capillary pressure increase, while the decrease in elastic properties is mainly a consequence of micro-cracking.

In this context, the originality of our contribution is (1) to check the validity of the linear, isotropic poroelastic approach with single porosity, full de-saturation and infinitesimal transformations for a model cement-based material, and (2) to identify the effect of heat treatment and hydrostatic loading upon the main poroelastic properties K_b and K_s (or K_b and b) identified for the model material. The paper is organised so as to explain accurately how K_b and K_s are identified from a simplified TPM approach (Section 2); then an original experimental methodology is developed (Section 3). It uses gas (and not water or ethanol) as an interstitial fluid, so as to avoid potential interactions with cement paste, and so as to saturate the pore network more quickly. It is usefully completed by ethanol saturation and mercury intrusion porosimetry. A simple statistical test quantifies whether changes in K_b and K_s with heat treatment are significant. Finally, results and analysis are proposed in Section 4.

2. Theory

2.1. Linear elasticity of fully-saturated isotropic porous media

In the following, for the sake of simplicity, we consider only fully-saturated elastic porous media with single porosity, no chemical interactions between fluid and solid, and it is also subjected to infinitesimal isothermal transformations. For anisotropy modelling and multiple-porosity approach, see for instance the short review proposed by Mian et al. [32]. For partial saturation, chemical and non-isothermal modelling, see O. Coussy [14].

A fully-saturated porous material is assumed to be the superposition of two independent overlapping continua, namely the solid skeleton (i.e. the material made of a solid matrix and of a *connected* pore network, both devoid of any free fluid) and the pore fluid [14,15]. In the present work, free water release from capillary pores is assumed to be fully achieved (see Section 3.2.1 for practical implementation), so that the material is fully air- (or gas-) saturated.

During the 1920's, K. Terzaghi provided a now classical effective stress theory [33] which is still widely used in soil mechanics, whereby the solid matrix grains are considered incompressible, and a uniform pore pressure p is accounted for:

$$\sigma_{eff} = \sigma_m + p \tag{1}$$

σ_{eff} is the stress *effectively* sustained by the porous material, while σ_m is the macroscopic mean stress (or hydrostatic stress)[1]. Indeed, Terzaghi found in particular that if the external mean pressure $\sigma_m = -P_{ext} < 0$ applied to a porous soil and the pore pressure $p > 0$ increase of the same amount (i.e. $p = P_{ext}$), the volume of the soil sample does not change [32].

In a later approach [13], M. Biot generalized Hooke's elastic behaviour law to porous materials by integrating the interstitial pore pressure effect; contrarily to soils, he considered that the solid skeleton is compressible due to interstitial pore pressure p, and proposed, in the case of an isotropic medium, a coefficient b to evaluate this effect, see [14,25]:

$$\sigma_m = K_b \varepsilon_v - b(p - p_0) \tag{2}$$

$$\phi - \phi_0 = b\varepsilon_v + \frac{(p - p_0)}{N} \tag{3}$$

[1] In soil mechanics convention, compressive stress is counted positive, hence the more usual formulation: $\sigma_{eff} = \sigma_m - p$.

where σ_m is the macroscopic mean stress (or hydrostatic stress), K_b is the porous medium drained bulk modulus, $\varepsilon_v = \Delta V/V$ is the volumetric strain (i.e. the relative volume variation), b is the Biot–Willis (or Biot) coefficient, $(p-p_0)$ is the pore pressure variation, $(\phi-\phi_0)$ is the normalized pore volume change (with ϕ_0 and ϕ denoting Lagrangian porosities), and N is the Biot skeleton modulus. b is shown to vary between initial porosity ϕ_0 and 1 which is the value for an incompressible solid matrix, so that Eq. (1) may be recovered for a soil: $\sigma_{eff} = \sigma_m + p = K_b\varepsilon_v$. For $\sigma_m = -P_{ext} < 0$ and $p = P_{ext} > 0$, the volumetric strain is zero, hence $\Delta V = 0$: the volume remains constant, as Terzaghi found out. Eq. (2) means that volumetric deformations of the porous medium are due to the contribution of both internal pore pressure (weighted by the solid skeleton relative compressibility represented by b), and applied mean stress σ_m. Eq. (3) means that the change in normalized pore volume is due to both skeleton volumetric deformations and pore pressure effect. Moreover, Nur and Byerlee [34] have shown analytically that:

$$b = 1 - \frac{K_b}{K_s} \tag{4}$$

where K_b is the skeleton bulk modulus and K_s is the solid matrix bulk modulus (i.e. solid without interconnected pores). Additionally, $1/N = (b-\phi_0)/K_s$, see [25]. The TPM approach has been generalised to any stress tensor (σ_{ij}), and associated with a Thermodynamics basis, by O. Coussy [14].

Physical interpretation

Drained modulus K_b provides an evaluation of the solid skeleton compressibility. In the case of a cement-based material, K_b accounts for the compressibility of the calcium silicate hydrates (C–S–H) mainly, added to that of the aggregates (and various other phases, such as Portlandite $Ca(OH)_2$, hydrated aluminates, or ettringite), and of the connected and non connected pore networks. Complementarily, the *apparent* solid matrix bulk modulus K_s accounts for the compressibility of the solid skeleton, mainly composed of C–S–H, small $Ca(OH)_2$ crystals and non connected porosity [14]. When heating up to 400 °C, it is essentially C–S–H which are decomposed in the solid skeleton (with ettringite), so as to release structural bound water [35]. This is thought to increase C–S–H rigidity and also C–S–H tendency to collapse at the microstructural scale.

2.2. Consequences: experimental identification of poro-elastic parameters

For a given porous material, particular stress paths may be followed in order to identify poro-elastic parameters easily. The most useful information is certainly deduced from hydrostatic compressibility tests [12,14], whereby confining pressure P_c is applied to the material, so that $\sigma_m = (1/3)\sigma_{ii} = -P_c$. Subsequently, it is readily seen from Eqs. (2) and (4) how K_b and b (or rather K_b and K_s) may be identified.

2.2.1. Bulk modulus K_b

If pore pressure p (also called interstitial pressure P_i hereafter) remains constant while confining pressure is changed by ΔP_c, K_b is derived from the following:

$$K_b = -\frac{\Delta P_c}{\Delta\varepsilon_v} \Leftrightarrow \Delta\varepsilon_v = -\frac{\Delta P_c}{K_b} \tag{5}$$

where $\Delta\varepsilon_v$ is the change in volumetric strain due to the change in confining pressure ($\Delta\varepsilon_v < 0$ when confining pressure is increased). There are two methods to maintain P_i at a constant value: either the sample is freely drained at both ends so that P_i remains equal to atmospheric pressure P_{atm} (zero relative pressure), or small amounts of pore fluid are expelled from the downstream side of the sample so that P_i is kept to a given constant value [24]. In the present study, the sample is drained freely at both ends while confining pressure is varied.

From (ε_v, P_c) data, a *secant* drained bulk modulus K_b is identified upon unloading. At each confinement of 10 MPa (or 12 MPa), 15 MPa, 20 MPa and 25 MPa, an unloading phase of $\Delta P_c = 5$ MPa is performed. In this domain, the evolution of (ε_v, P_c) data is almost linear. This procedure avoids re-opening hugely the micro-cracks, and solicitates mainly elastic energy release. Drained bulk modulus K_b is then determined as the slope of the linear interpolation between the (ε_v, P_c) experimental points measured during this unloading phase.

2.2.2. Solid matrix bulk modulus K_s

As O. Coussy [14] recalls, when confining pressure is varied of the same amount as the interstitial pore pressure, i.e. $\Delta P_c = \Delta P_i$, the measured volumetric strain $\Delta\varepsilon_v$ of the sample is exactly equal to the solid matrix volumetric strain $\Delta\varepsilon_v^s$. The solid matrix bulk modulus K_s is therefore deduced from:

$$K_s = -\frac{(\Delta P_c = \Delta P_i)}{(\Delta\varepsilon_v = \Delta\varepsilon_v^s)}. \tag{6}$$

Yet, imposing experimentally $\Delta P_c = \Delta P_i$ is quite delicate, all the more so as gas is used as interstitial fluid. Indeed, available ΔP_i are quite low compared to ΔP_c which is imposed through oil confinement. Therefore, such a loading path has not been chosen. Rather, a so-called *change in pore pressure* test [12], also referred to by O. Coussy [14], is carried out in two successive steps. First, confining pressure is varied under drained conditions so that $\Delta\varepsilon_{v1} = -(\Delta P_c/K_b)$ is measured. Secondly, the pore pressure is varied by $\Delta P_i < \Delta P_c$ while confining pressure is held constant. This second step leads to a volumetric strain $\Delta\varepsilon_{v2}$, which varies linearly with ΔP_i, so that a modulus H may be derived from:

$$\Delta\varepsilon_{v2} = \frac{\Delta P_i}{H} \tag{7}$$

In this case, $\Delta\varepsilon_{v2} > 0$ when interstitial pressure is increased. This linear relationship is still assumed valid when extrapolated to the case when $\Delta P_c = \Delta P_i$. Finally, after the first drained loading step followed by the second undrained step extrapolated to $\Delta P_c = \Delta P_i$, the porous material has deformed by $\Delta\varepsilon_v = -(\Delta P_c = \Delta P_i)/K_s = \Delta\varepsilon_{v1} + \Delta\varepsilon_{v2} = -(\Delta P_c/K_b) + (\Delta P_i/H)$, so that finally:

$$\frac{1}{K_s} = \frac{1}{K_b} - \frac{1}{H} \tag{8}$$

In practice, and contrarily to K_b, which is determined during P_c unloading phases, modulus H is determined during P_i loading phases.

2.2.3. Biot's coefficient

Biot's coefficient b is a key parameter in poro-mechanical couplings, and extensive investigations have been conducted towards its determination. It may be obtained through a direct experimental method, see [36,24], whereby P_c is kept constant and interstitial pressure is varied by ΔP_i. This experiment, which corresponds exactly to the second step of the *change in pore pressure* test, provides:

$$b = K_b\frac{\Delta\varepsilon_{v2}}{\Delta P_i} \tag{9}$$

i.e. $b = K_b/H$. b being derived from the same *change in pore pressure* test as K_s, this expression corresponds to the combination of Eqs. (4) and (8).

2.2.4. Applicability to cement-based materials

It is to be noted here that while the solid skeleton of mortars (or cement pastes) exhibits strong heterogeneities (e.g. sand aggregates among cement paste, and anhydrous clinker surrounded by C–S–H at a lower scale), Eqs. (4) and (8) are valid provided the solid phase is considered homogeneous. In our experiments, we evaluate compressibility moduli (K_b, H and K_s) from average strain gauge and pressure

measurements, so that the solid skeleton is assumed homogeneous at the macroscopic scale involved for these measurements. Strain gauge dimensions are chosen in order to be representative of the material surface strain at the macroscopic scale, and pressure measurements are taken as the average pressure inside the pore network, by using a manometer placed in the vicinity of both sample ends, see Section 3 for practical implementation. In brief, our measurements relate to macroscopic poroelastic properties, so that the solid skeleton heterogeneities at the microscopic scale (and below) are considered as averaged.

3. Experimental methodology

3.1. Materials

A normalized mortar with a water-to-cement (W/C) ratio of 0.5 was made using 0/4 mm normalized sand (from Leucate, France) and Type II Portland cement referenced CEM II/B-M (LL-S) 32.5R. European Standard EN197-1/2000 describes its composition as comprising 65–79% clinker, 21–35% calcite and 0–5% secondary constituents. The mass proportion of mortar constituents is given in Table 1. This mortar was used for a wide variety of studies in our laboratory, see for instance [37–40,12], and it may be easily reproduced by other laboratories for comparison and/or further studies. Ulm et al. [25] use a very similar (W/C)=0.5 model mortar, except that it is composed of Type I Portland cement.

The necessary amount of mortar to achieve the whole study was cast in a beam formwork of 50 cm length and 15×25 cm^2 cross-sectional area. The mortar surface in contact with air was preserved from desiccation with plastic sheets, until stripping after 48 h. Then, the beam was immersed for 6 months in lime-saturated water at a constant temperature of 20 °C, in order to eliminate the effects of thermal and endogenous shrinkages, and to achieve proper mortar maturation [41,42]. Afterwards, cylindrical samples of 37 mm diameter and 70 mm height were cored and carefully ground to obtain a plane geometry for both end surfaces.

3.2. Experimental procedures

3.2.1. Preliminary thermal cycling

The effect of thermal treatment is evaluated by comparison with a reference state for the material. Oven-heated mortar at a temperature of 60 °C until constant mass was chosen as the reference state. In accordance with former experimental studies performed in our laboratory [37,43], this procedure is considered to provide a reference state because it allows evaporation of free water from the capillary macropores, without significant effect upon the C–S–H gel [44]. In the following, the dried material state (after oven-heating at 60 °C) is referred to as the *intact* or *reference* mortar state.

After initial drying to the reference state, samples were heated up either to 105, 200, 300, or 400 °C, while a number was kept in the intact reference state for subsequent testing. For each thermal treatment, a temperature rate of 20 °C/h, situated in the low range as in [5,45], was imposed during heating and subsequent cooling, using a programmable oven (Nabertherm™, Model LH 60/12, Germany). Cooling was programmed after 1 h temperature stabilisation at 105, 200, 300 or 400 °C. As recommended by RILEM, see [7], the low temperature rate and the stabilisation step both aim at ensuring a homogeneous temperature state in the sample, i.e. to prevent temperature gradients, thermal shock, and sample macro-cracking, see also [46].

Table 1
Mass proportion of mortar constituents for a (W/C) ratio of 0.5

Constituent	Mass (kg)
Cement	450
Normalized sand	1350
Water	225

Water loss after heat cycling was measured by weighing to an accuracy of 0.01 g. Prior to heating, all samples have an initial average mass of 159.37 g ± 1.35. Samples heated up to 300 °C loose by 2.4% ± 0.1 of their initial average mass, and those heated up to 400 °C loose 3.3% ± 0.2 of their initial average mass. This result is in accordance with the literature. For instance, a (W/C)=0.5 high performance concrete (HPC) looses by 4% of its initial mass when heated up to 300 °C (respectively by 6% of its initial mass when heated up to 400 °C), see [47].

3.2.2. Ethanol saturation and mercury intrusion porosimetry

Both ethanol saturation and mercury intrusion porosimetry procedures were performed on samples preliminary dried at 60 °C until mass stabilisation, in order to remove free water from the interconnected porosity. During the ethanol saturation procedure, each sample was immersed in ethanol inside a vacuum chamber until mass stabilisation. The difference between dry mass and full ethanol saturation mass provided the amount m_p of ethanol filling the interconnected pores. The pore volume V_p is deduced from ethanol density ($\rho_{ethanol}$=0.791 g/cm^3): $V_p = m_p/\rho_{ethanol}$. ϕ is obtained after sample volume V_{total} measurement, as $\phi = V_p/V_{total}$.

MIP tests were performed on a representative 1 cm^3-sized sample for each of the five mortar conditions: 60 °C reference drying, 105 °C, 200 °C, 300 °C and 400 °C heating/cooling cycle, using a MICROMERITICS® AutoPore IV 9500 device. The sample was placed inside a hermetic chamber; vacuuming was performed in order to remove air and potential residual water from the sample, then mercury liquid pressure was increased step by step up to 200 MPa (each step lasted 20 sec) so that greater and greater volumes entered the material interconnected pores. Laplace equation: $P = (2\gamma\cos\theta/r)$, where γ=0.485 N/m is the mercury surface tension, θ=130° is the mercury contact angle, provided the average pore radius r down to which mercury had intruded the sample at given applied pressure P. In parallel, the intruded mercury amount, determined by weighing (with ρ_{Hg}=13.5335 g/ml) quantified the intruded pore volume at given P.

3.2.3. Poro-mechanics experimental devices and measurement accuracy

Triaxial experiments were carried out using a hydrostatic loading cell, see Fig. 1. Prior to being placed inside the triaxial cell, the sample was jacketed inside a protective Viton® membrane. A confining pump (Gilson® 303) was used to hold the required confining oil pressure level P_c constant. Confining pressure values were recorded using a Bourdon dial pressure gauge with an accuracy of ±(1/4) MPa (corresponding to half the card face smallest graduation). Interstitial pressure values were recorded by two Kobold® digital pressure gauge transducers located each on one sample side, each with an accuracy of ±0.1 MPa. 99% pure inert argon gas was used as the interstitial fluid, in order to avoid potential chemical reactions with the sample material. Using gas to perform poro-elastic measurements is one major originality of the experimental procedure. Indeed, gas allows faster fluid saturation of the pore network, and is sensibly less reactive with cement-based materials than water.

Four strain gauges were glued on the sample surface. They were all placed around the sample median plane, two longitudinally and two transversally. Corresponding longitudinal and transversal strain values (ε_1, ε_2, ε_3 and ε_4) were recorded using a Labview® (National Instrument™) conditioning system with an accuracy of $\pm 10^{-6}$. After setting given confinement and interstitial pressure values, a stabilisation time of several minutes was observed prior to strain recording. All poro-mechanical tests have taken place in a temperature-controlled room at 22 °C, in order to avoid possible variations of confining pressure, interstitial pressure, or even strain gauge values with temperature. The maximum difference in gauge response was on the order of 6.5% at 25 MPa for drained tests, and 4% at 8 MPa during *change in pore pressure* tests. This means that the material response may be considered isotropic, so that the

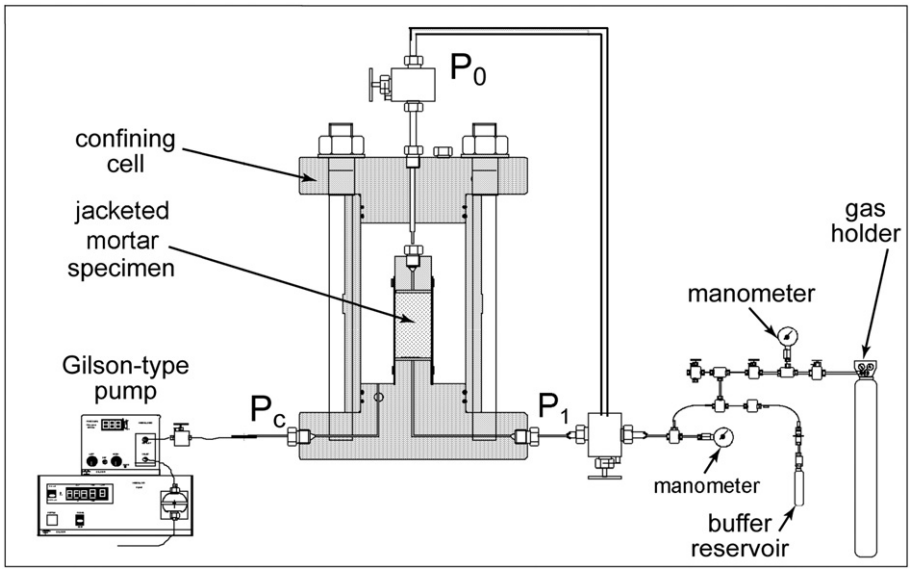

Fig. 1. Experimental device used for the poromechanical tests, derived from that used in [24]. The main originality here is to apply an identical gas pressure on both sample sides so as to saturate it more quickly.

volumetric strain was directly evaluated as threefold the average gauge strain:

$$\varepsilon_v = 3\times\frac{\varepsilon_1+\varepsilon_2+\varepsilon_3+\varepsilon_4}{4} \quad (10)$$

3.2.3.1. Experimental procedure. For the *change in pore pressure* test, interstitial pressure was set to a given value as follows. First, confining pressure was set to the desired value using the confining pump, and let to stabilise for about half an hour. Then, argon gas was let to flow through the buffer reservoir down to both upstream and downstream sample sides at pressure $P_0=P_1=P_i>P_{atm}$, see Fig. 1. For drained tests, $P_0=P_1=P_{atm}$ at all times.

3.3. Statistical analysis

Despite disposing of only two (or three) experimental values for each material and heat treatment condition, poroelastic parameters K_b and K_s were compared using a statistical test such as in [48], in order to determine whether any of the heating/cooling cycles leads to significant differences from the initial reference state. To this purpose, average values $K_{b\ mean}$ and $K_{s\ mean}$ were evaluated from the two tests performed at each given temperature, e.g. $K_{b\ mean}(T)=(K_{b1}+K_{b2})/2$ for K_b, after cycling up to T=60 °C (reference state), 105, 200, 300 or 400 °C. At each temperature, standard deviation was also evaluated classically, e.g. as: $\sigma_b(T)=\sqrt{\frac{1}{2}*\left((K_{b1}-K_{b\,mean})^2+(K_{b2}-K_{b\,mean})^2\right)}$ for two drained tests on K_b. The statistical test assumes that if an infinite number of poromechanical tests were performed, the distribution of experimental data (i.e. the number of tests providing a given K_b or K_s value, also called the *probability density*) would follow a Gaussian evolution. The statistical test aimed at determining whether the values of K_b (respectively K_s) differ significantly before or after heat treatment. The difference between K_{bA} (population A, e.g. tests at the reference state) and K_{bB} (population B, e.g. tests after a heating/cooling cycle up to 300 °C) is considered statistically significant if the intervals $[(K_{b\ mean}-2*\sigma_b);\ (K_{b\ mean}+2*\sigma_b)]$ (also called *boxes*), evaluated for each population A and B, do not overlap. For each population, such an interval corresponds to 95% of the possible tests that might be performed. An even more constraining statistical test imposes no overlapping to 99% of the two test populations, i.e. no overlapping to intervals of the form $[(K_{b\ mean}-4*\sigma_b);\ K_{b\ mean}+4*\sigma_b]$. Both 95% and 99% statistical tests were performed.

4. Results and analysis

After presenting porosity results, poro-mechanical test results are divided in two successive parts in order to highlight, first, the effect of temperature cycling, and, second, the effect of confining pressure upon poroelastic properties.

4.1. Ethanol saturation and mercury intrusion porosimetry results

Fig. 2 compares porosity results given either by MIP (one sample tested) or through the ethanol saturation method (three samples tested). Despite porosity decreases by 1% between 105 and 200 °C

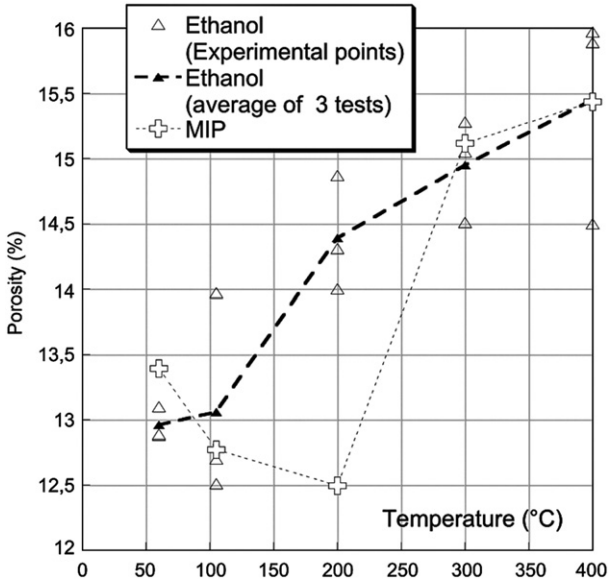

Fig. 2. Ethanol saturation and mercury intrusion porosimetry results. Porosity is evaluated as the average of three tests for the ethanol saturation method.

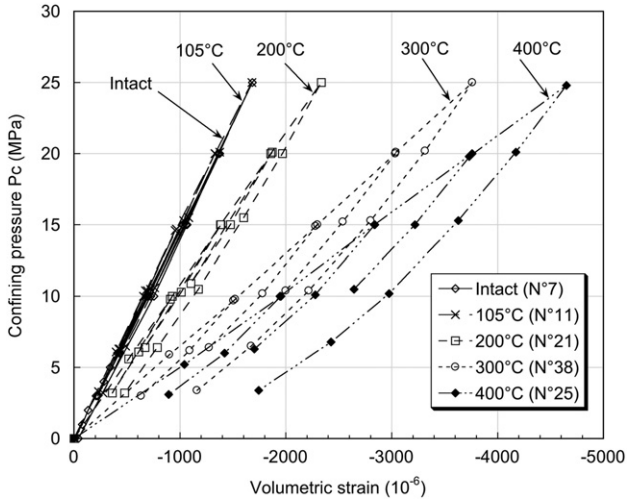

Fig. 3. Raw drained test data (ε_v,P_c) for one representative sample of intact and heat-treated mortars.

with MIP, ethanol saturation results are in favour of a regular, monotonous increase of porosity with heat-treatment. In particular, after a 400 °C heat-treatment, porosity increases by about 2.5%, which represents 19.2% of the initial porosity.

4.2. Evidence of microstructure evolutions from drained triaxial tests

For intact and heat-treated mortars up to 105 °C, the (ε_v,P_c) data correspond to a linear elastic behaviour until brittle failure, see Figs. 3 and 4. This means that no noticeable plastic strains are to be accounted for in the mortar samples. On the opposite, for samples heated up to 200, 300 and 400 °C, (ε_v,P_c) behaviours are highly non linear and ductile. Observed under monotonously increasing confinement, such non linearity corresponds to the development of plastic strains, which are a consequence of thermal damage. Thermal damage manifests itself as various micro-cracking mechanisms, see Section 4.3.1. Micro-cracking induces gradual failure of solid skeleton bridges (or trabecules), such as proposed in [49]. This effect is amplified with increasing heat treatment temperature, which is very probably linked with increasing micro-crack amount. Indeed, mortars heat-treated up to 200 °C and above are not only notably more compressible than the intact and 105 °C heat-treated mortars, but their compressibility, evaluated at given confining pressure as the secant bulk modulus K_b, is smaller and smaller with increasing heat treatment temperature, see Fig. 5. For instance, at 25 MPa confinement, the 300 °C heat-treated mortar deforms 2.4 more than the intact mortar, while the 400 °C heat-treated mortar deforms about three times more than the intact mortar.

In addition to their linear and reversible behaviour, intact and heat-treated mortars up to 105 °C have a constant K_b, independent of confining pressure increases, see Fig. 5 and Tables 2 and 3. At intact state, K_b values are in good accordance with previous study by Skoczylas et al. [12], see Table 7. On the contrary, each mortar heat-treated up to 200, 300 and 400 °C displays a noticeable increase of drained bulk modulus K_b with increasing confining pressure, see Figs. 4(A), (B), 5 and Tables 4–6. For each heat-treatment temperature above 105 °C, the increase in K_b with P_c is attributed to some collapse of the porous network, so that the solid skeleton compactness is greater, as proposed by Kherbouche [49] in the case of calcite.

Table 3
Variation of poroelastic properties due to confining pressure (samples heat-treated up to 105 °C)

Sample	No. 11				No. 19			
P_c (MPa)	K_b (MPa)	H (MPa)	K_s (MPa)	b	K_b (MPa)	H (MPa)	K_s (MPa)	b
12	16,270	26,896	41,182	0.605	15,948	24,822	44,609	0.642
15	16,092	26,140	41,864	0.616	16,291	25,245	45,931	0.645
20	15,946	27,232	38,476	0.586	15,838	–	–	–
25	16,212	26,882	40,845	0.603	16,265	25,780	44,068	0.631

Finally, the following should be highlighted. At given heat treatment temperature above 105 °C, the tangent bulk modulus $K_{b\ tangent}$, evaluated as the tangent to the (ε_v,P_c) curve at given P_c, decreases regularly with increasing P_c, see Fig. 3, while the secant bulk modulus K_b, determined during a ΔP_c=5 MPa unloading phase, increases with increasing P_c. Both evolutions are consequences of thermal damage. On the one part, thermal damage weakens the solid skeleton: this is observed as plastic straining upon increasing confinement. On another part, thermal damage induces greater solid skeleton compactness after pore network collapse and solid bridges failure, which induces greater bulk modulus K_b when evaluated upon a ΔP_c=5 MPa unloading.

4.3. Influence of thermal cycling upon K_b, K_s and b

As displayed Fig. 5, drained bulk modulus K_b decreases notably with increasing heat-treatment temperature T. Tables 7 and 8 show that, at an identical confining pressure P_c=15 MPa, K_b equals to 16,125 MPa on average for an intact mortar and it is similar at a value of 16190 MPa for a 105 °C heat-treated mortar. 95 and 99% possible test population intervals overlap: there is no statistically significant difference in K_b for intact or 105 °C heat-treated mortar. On the opposite, K_b starts to decrease significantly from 200 °C heat-treatment with an average value of 12850 MPa. For a mortar heat-treated up to 300 °C, K_b reduces to almost half the intact one, with an average value of 9840 MPa. For a mortar heat-treated up to 400 °C, K_b is smaller, with an average value of 9080 MPa, yet K_b remains inside the same Gaussian interval as for a 300 °C heat–treatment. K_b is significantly lower than its intact (or 105 °C heat-treatment) value after a 200 °C heat-treatment, then after a 300 to 400 °C heat–treatment. This progressive and significant decrease in K_b at given P_c is attributed to thermal damage, and in particular to mortar progressive micro-cracking. This is concomitant with an increase in connected porosity, see Fig. 2, and a coarsening of pore sizes that MIP shows (not displayed in this paper).

4.3.1. Evidence of mortar thermal damage and micro-cracking

Mortar (and concrete) may be considered a non-homogenous two-phase solid composed of a porous cement paste skeleton mixed with aggregate particles. When mortar is subjected to elevated temperatures,

Table 2
Variation of poroelastic properties due to confining pressure (intact samples)

Sample	No. 7				No. 8				No. 24			
P_c (MPa)	K_b (MPa)	H (MPa)	K_s (MPa)	b	K_b (MPa)	H (MPa)	K_s (MPa)	b	K_b (MPa)	H (MPa)	K_s (MPa)	b
12	15,370	260,30	37,531	0.590	17,544	26,926	50,351	0.652	15,974	24,838	44,761	0.643
15	15,613	25,271	40,853	0.618	17,241	26,287	50,101	0.656	15,522	23,825	44,540	0.652
20	15,686	–	–	–	17,857	27,856	49,747	0.641	15,238	–	–	–
25	15,576	24,512	42,726	0.635	17,794	28,359	47,763	0.627	16,181	24,500	47,654	0.660

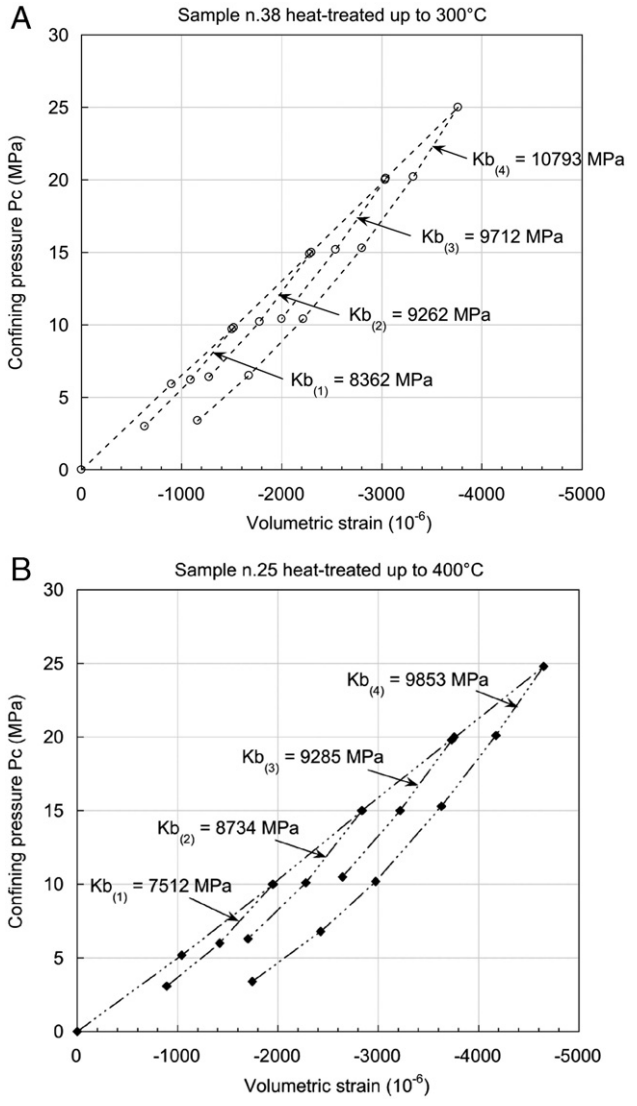

Fig. 4. Raw drained test data (ε_v,P_c) (A): for Sample n.38 heat-treated up to 300 °C; (B): for Sample n.25 heat-treated up to 400 °C. Each of the four successive ΔP_c = 5 MPa unloading phases is used to determine K_b at 10 (or 12), 15, 20 or 25 MPa.

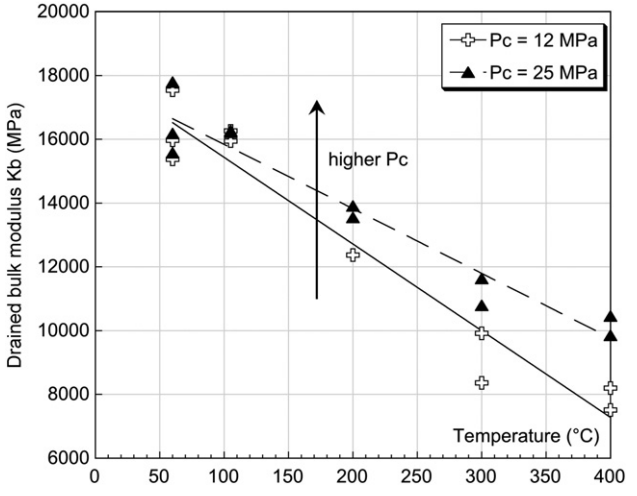

Fig. 5. Drained bulk modulus K_b decreases with increasing heat-treatment temperature and, from 200 °C onwards, K_b increases with increasing confining pressure P_c.

Table 4
Variation of poroelastic properties due to confining pressure (samples heat-treated up to 200 °C)

Sample	No. 21				No. 22			
P_c (MPa)	K_b (MPa)	H (MPa)	K_s (MPa)	b	K_b (MPa)	H (MPa)	K_s (MPa)	b
12	12,375	17,440	42,610	0.710	–	–	–	–
15	12,533	18,385	39,374	0.682	13,175	19,627	40,078	0.671
20	12,846	18,785	40,632	0.684	13,307	–	–	–
25	13,550	20,191	41,197	0.671	13,913	22,581	36,245	0.616

Table 5
Variation of poroelastic properties due to confining pressure (samples heat-treated up to 300 °C)

Sample	No. 14				No. 38			
P_c (MPa)	K_b (MPa)	H (MPa)	K_s (MPa)	b	K_b (MPa)	H (MPa)	K_s (MPa)	b
12	9917	–	–	–	8362	–	–	–
15	10,412	12,999	52,318	0.801	9262	11,297	51,417	0.820
20	10,811	14,785	40,222	0.731	9712	–	–	–
25	11,639	16,526	39,359	0.704	10,793	14,618	41,248	0.738

Table 6
Variation of poroelastic properties due to confining pressure (samples heat-treated up to 400 °C)

Sample	No. 15				No. 25			
P_c (MPa)	K_b (MPa)	H (MPa)	K_s (MPa)	b	K_b (MPa)	H (MPa)	K_s (MPa)	b
12	8202	–	–	–	7512	8432	68,849	0.891
15	9430	10,954	67,780	0.861	8734	10,019	68,098	0.872
20	9891	12,560	46,546	0.788	9285	11,439	49,309	0.812
25	10,462	13,474	46,801	0.776	9853	12,881	41,914	0.765

thermal damage is expected to be the result of several phenomena, such as, in particular, increasing mismatch of expansion/shrinkage between paste and aggregates, strength-weakening decomposition of hydrates,

Table 7
Values of K_b and K_s for intact mortar or after thermal treatment up to 105 or 200 °C, under an identical confining pressure of 15 MPa

Sample no. or statistical parameter	Drained bulk modulus K_b in MPa	Matrix bulk modulus $K_s = \left(\frac{1}{K_b} - \frac{1}{H}\right)^{-1}$ in MPa
No. 7 (intact)	15,613	40,853
No. 8 (intact)	17,241	50,101
No. 24 (intact)	15,522	44,540
Average value ± deviation to the average expressed in %	16,125 ± 7%	45,165 ± 10%
Gaussian interval for 95% cases (average ± 2 standard deviation)	[14,545–17,705]	[37,563–52,767]
Gaussian interval for 99% cases (average ± 4 standard deviation)	[12,965–19,285]	[29,961–60,369]
Reference [12]—No. 1 (intact)	*17,700*	*42,400*
Reference [12]—No. 2 (intact)	*16,900*	*36,500*
No. 11 (treated up to 105 °C)	16,092	41,864
No. 19 (treated up to 105 °C)	16,291	45,931
Average value ± deviation to the average expressed in %	16,192 ± 0.6%	43,898 ± 4.6%
Gaussian interval for 95% cases (average ± 2 standard deviation)	[15,993–16,391]	[39,832–47,964]
Gaussian interval for 99% cases (average ± 4 standard deviation)	[15,794–16,590]	[35,766–52,030]
No. 21 (treated up to 200 °C)	12,533	39,374
No. 22 (treated up to 200 °C)	13,175	40,078
Average value ± deviation to the average expressed in %	12,854 ± 2.5%	39,726 ± 0.9%
Gaussian interval for 95% cases (average ± 2 standard deviation)	[12,212–13,496]	[39,022–40,430]
Gaussian interval for 99% cases (average ± 4 standard deviation)	[11,570–14,138]	[38,318–41,134]

Table 8
Values of K_b and K_s after thermal treatment at 300 and 400 °C, under an identical confining pressure of 15 MPa

Sample no. or statistical parameter	Drained bulk modulus K_b in MPa	Matrix bulk modulus $K_s = \left(\frac{1}{K_b} - \frac{1}{H}\right)^{-1}$ in MPa
No. 14 (treated up to 300 °C)	10,412	52,318
No. 38 (treated up to 300 °C)	9262	51,417
Average value ± deviation to the average expressed in %	9837 ± 6%	51,868 ± 0.9%
Gaussian interval for 95% cases (average ± 2 standard deviation)	[8687–10,987]	[50,968–52,768]
Gaussian interval for 99% cases (average ± 4 standard deviation)	[7537–12,137]	[50,068–53,668]
No. 15 (treated up to 400 °C)	9430	67,780
No. 25 (treated up to 400 °C)	8734	68,098
Average value ± deviation to the average expressed in %	9082 ± 4%	67,939 ± 0.2%
Gaussian interval for 95% cases (average ± 2 standard deviation)	[8386–9778]	[67,621–68,257]
Gaussian interval for 99% cases (average ± 4 standard deviation)	[7690–10,474]	[67,303–68,575]

and dehydration-induced cracks [50,9]. Indeed, aggregates always expand upon heating whereas cement paste expands until 150 °C, then shrinks at higher temperatures. As a consequence, micro-cracks occur with a possible effect on porosity and permeability [51]. For instance, for a normalized mortar (W/C = 0.5) of identical constituents as ours, M. Lion et al. [43] show a very clear increase in permeability from 200 °C heating. This is attributed to mortar micro-cracking, which becomes connected at this temperature. Moreover, strain incompatibilities between cement paste and aggregates may be caused by rigidity differences. Since aggregates are acting as rigid inclusions, cement paste deformations will be prevented by aggregates, which leads to micro-cracking [52,53]. Fu et al. [10] report three typical mismatch-induced cracks (radial cracks, tangential cracks and inclusion cracks) around a sand aggregate in a mortar heated at 300 °C.

As for them, dehydration-induced cracks have been attributed to the thermal mismatch of expansion/shrinkage among the different cement paste hydration products [54]. At the cement paste level, the main reason for dehydration-induced cracks and shrinkage, which occur with temperature increase, is the loss of free or bound water [43,55]. Free water is acknowledged fully evaporated from the paste above 105 to 145 °C [35,56]. Up to a level of 400 °C, which is the maximum heat–treatment temperature used in this study, Portlandite $Ca(OH)_2$ is not considered decomposed, whereas the main cement paste constituents (in mass), namely calcium silicate hydrates (C–S–H) are reputed to release all bound water molecules [35,56].

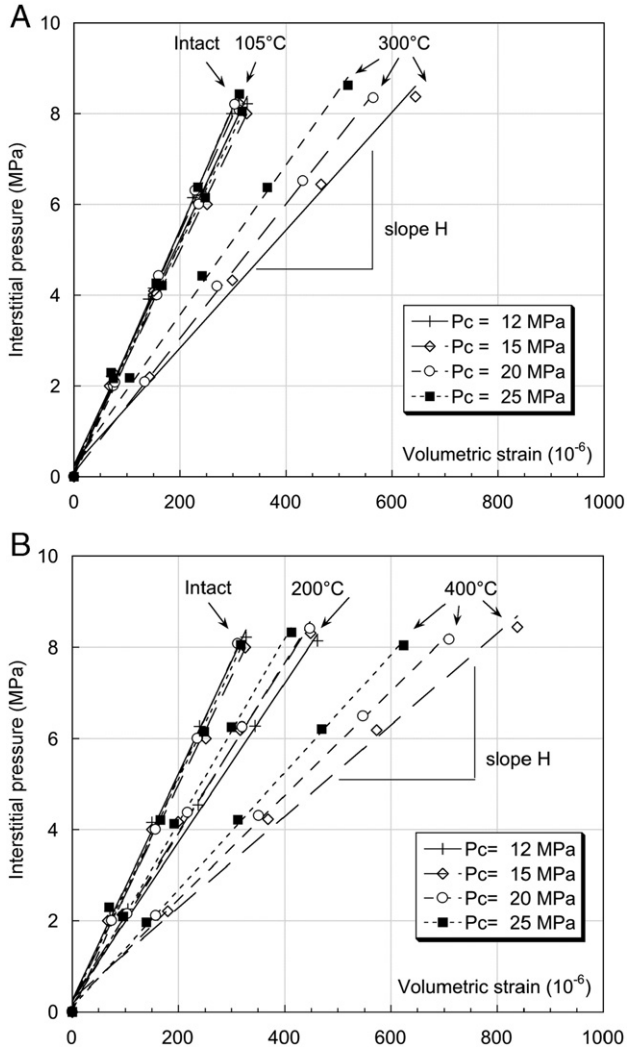

Fig. 6. Raw *change in pore pressure* test data (ε_v,P_i) for (A): intact and heat-treated mortars up to 300 °C; (B): intact and heat-treated mortars up to 400 °C. The decrease in H with increasing heat-treatment temperature is clear, as well as its relative increase with increasing P_c.

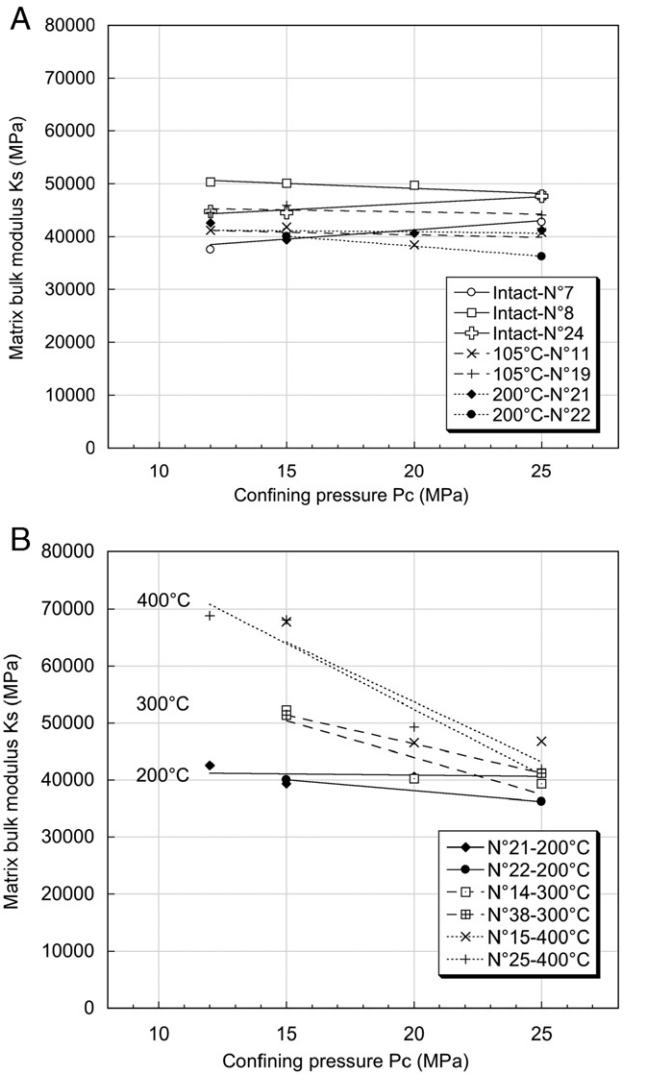

Fig. 7. Solid matrix bulk modulus K_s as deduced from drained and *change in pore pressure* test results (A): for intact and heat-treated mortars up to 200 °C; (B): for mortars heat-treated up to 400 °C. A clear decrease in K_s with increasing confinement is noticed from 300 °C heat-treatment.

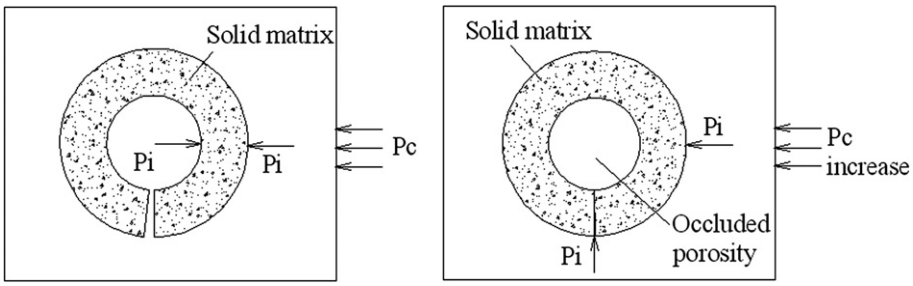

Fig. 8. Interpretation of test results: (1) left figure: the porous material is assumed to contain a number of micro-cracks, or fine canals, connected to pores; (2) right figure: when confining pressure P_c increases, some micro-cracks (or fine canals) close, which closes access to some pores. Those pores get occluded and hence, are included in the solid matrix when measuring K_s. A solid matrix with occluded porosity is more compressible than a purely solid matrix, therefore, K_s is smaller in the former case.

After *change in pore pressure* tests, values for matrix bulk modulus K_s are deduced from modulus H values, see Fig. 6(A), (B). Contrarily to drained bulk modulus K_b, matrix bulk modulus K_s increases with heat-treatment temperature at low confinement levels (i.e. below 15 MPa), see Fig. 7(A) and (B). This is most noticed for mortars heat–treated up to 300 °C and 400 °C. The difference in K_s for intact, 105°, and 200 °C heat-treated mortars is not statistically significant, whereas it is with mortar heat–treated up to 300 °C, see Tables 7 and 8. There is also a statistically significant increase in K_s when comparing all mortars to that heat-treated up to 400 °C. Our interpretation, limited to low confining pressures (15 MPa at most) is as follows. As micro–cracks have been created during thermal treatment, originally occluded porosity in the solid matrix may have become connected. This is correlated with measurements of connected porosity increase, see Section 4.1 and Fig. 2. As a consequence, the solid matrix contains less occluded porosity, so that it becomes less compressible (i.e. more rigid), wherefore K_s increases. It will be shown hereafter that this effect is reversed for higher confining pressures, whereby micro–cracks get closed and entrap some pores into the solid matrix (i.e. occluded porosity increases).

Recalling that Biot's coefficient b is deduced from both K_b and K_s, a statistically significant variation is also shown for b (yet not displayed in this paper). Indeed, Biot's coefficient b gets closer and closer to 1 with increasing heat–treatment temperature with an upper limit at ca. 0.89, as the mortar skeleton degrades more and more towards a granular, non cohesive, microstructure.

4.4. Influence of confining pressure upon K_s and b

As stated above (Fig. 6(A) and (B)), for intact and heat–treated mortars up to 105 °C, modulus H does not change significantly with confining pressure, so that matrix bulk modulus K_s and Biot's coefficient b remain unchanged when P_c increases. On the opposite, modulus H increases with confining pressure for samples heat-treated up to 200 °C, 300 °C and 400 °C. For mortars heat–treated up to 200 °C, Biot's coefficient b remains in the [0.61–0.71] range proposed by Ulm et al. [25], yet for the C–S–H phase at a lower scale.

Conclusions are slightly different for matrix bulk modulus K_s, because while K_s is not significantly influenced by confining pressure variations for mortars heat-treated up to 200 °C, see Fig. 7(A) and (B), K_s decreases significantly with increasing P_c from 300 °C heat-treatment. Indeed, K_s integrates the effects of both H and K_b. The decrease in K_s with confinement is attributed to a loss of connection of part of the porous system, due to micro–cracks closure when confining pressure increases, see Fig. 8 .The more occluded porosity exists in the solid matrix, the more compressible the solid matrix becomes and the smaller the value of K_s is. In other words, when confining pressure P_c increases, parts of the porous system loose connection due to the closure of connecting channels (such as micro–cracks). As the solid matrix includes more occluded porosity, matrix bulk modulus K_s gets smaller. As mentioned by Coussy [14], "it is worthwhile to note that a divergence of K_s from the bulk modulus of the solid "grains" forming the matrix will infer the existence of an occluded porosity" (p79). Due to our experimental procedure (i.e. *change in pore pressure test* at a macroscopic scale), K_s corresponds to an *apparent* bulk modulus for the mortar solid matrix, i.e. solid grains and occluded porosity, contrarily to Cheng et al. [57]. Indeed, in their micro-mechanics modelling approach, Cheng et al. [57] account

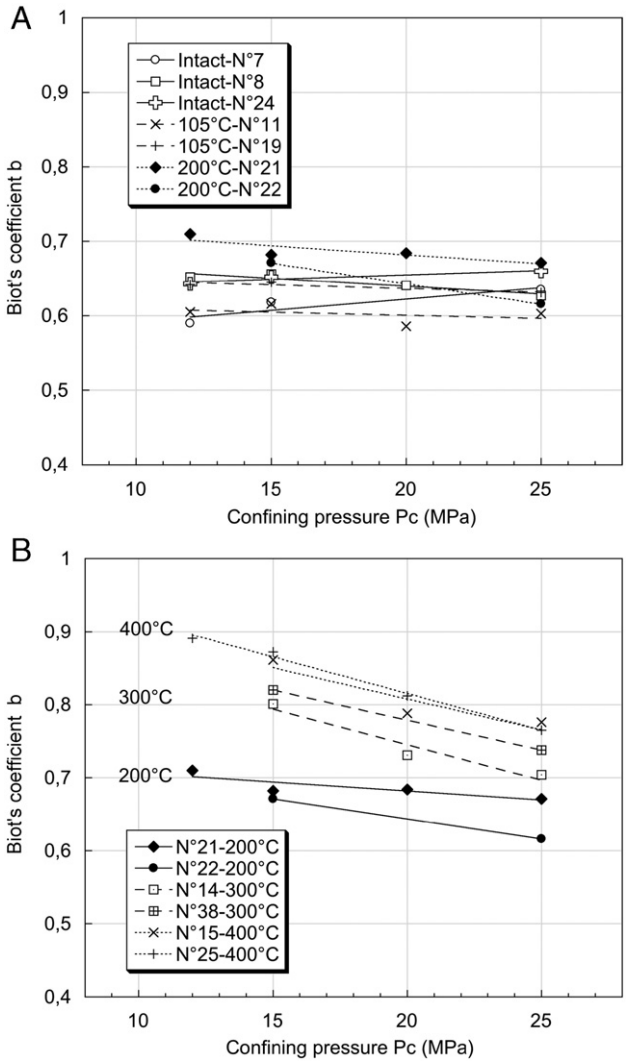

Fig. 9. Biot's coefficient b with increasing confinement, as deduced from drained and *change in pore pressure* tests (A): for intact and heat-treated mortars up to 200 °C; (B): for mortars heat-treated up to 400 °C.

for porosity change associated to solid grain rearrangement, micro-anisotropy and micro–inhomogeneity of the solid phase. Also in favour of our interpretation, experimental results on Callovo–Oxfordian argillite are to be mentioned [58]. Biot's coefficient b and matrix bulk modulus K_s are shown to decrease with increasing axial stress. The authors interpretation is that when axial stress increases, a punching phenomenon may occur upon parts of the porous system, whereby meaning a loss of pore connection. This also means that more occluded porosity is created in the solid matrix due to increasing axial stress, so that the matrix bulk modulus K_s decreases.

If the material macroscopic behaviour law (Eqs. (2) and (3)) is to be interpreted physically, Biot's coefficient b means that the material deformation is not only governed by the deformation of the solid phases, but also by a change in porosity [14]. In good correlation with this, our results (Fig. 9 (A) and (B)) indicate that the creation of occluded porosity in the solid matrix, when increasing confining pressure, induces a decrease in Biot's coefficient b.

5. Conclusion

This contribution aimed at evaluating experimentally the effects of heat-treatment and confinement upon several poro-mechanical properties of a normalized mortar. Intact mortar (oven-dried at 60 °C until mass stabilisation) and heat–cycled mortars up to four different temperature levels (105 °C, 200 °C, 300 °C and 400 °C) were used. Drained bulk modulus K_b, solid matrix bulk modulus K_s and Biot's coefficient b were identified through drained or *change in pore pressure* tests and under different confining pressure levels (ranging from 12 to 25 MPa). Our main results are as follows:

- Drained test results for intact and heat-treated mortars up to 105 °C indicate that no noticeable micro–cracks may be accounted for, so that the (ε_v,P_c) behaviour is linear, elastic, reversible with brittle failure. Yet, for samples heat–treated up to 200 °C, 300 °C and 400 °C, the (ε_v,P_c) data are non linear and irreversible, which is attributed to thermal damage. Thermal damage degrades the solid skeleton mainly through the creation of various micro-cracks, down to the scale of cement paste phases, and increases connected porosity. For mortars heat–treated up to 300 °C and 400 °C mainly, secant bulk modulus K_b increases with confining pressure. This is attributed to pore network collapse, concomitant with increased solid skeleton compactness.
- At given confinement, drained bulk modulus K_b significantly decreases after a heating treatment above 105 °C. Again, this indicates thermal damage.
- On the opposite, the observed increase in K_s and Biot's coefficient b at low confinement is attributed to the reduction of occluded porosity in the solid matrix (due to interconnection by micro-cracks).
- For mortars heat–treated above 300 °C, matrix bulk modulus K_s and Biot's coefficient b significantly decrease when confining pressure increases. K_s being the solid matrix bulk modulus, it characterizes the compressibility of both cement paste solids and occluded porosity. When confining pressure increases, micro–cracks due to thermal damage close, so that parts of the porous network loose connection and get occluded inside the solid matrix. Therefore, the more occluded porosity the solid matrix contains, the more compressible it becomes, so that K_s decreases.

In further work, a thermodynamics-based macroscopic modelling approach will be tackled in order to represent and predict the effects of heat treatment and thermal damage upon mortar poro-elastic properties. Investigations of convective transport properties (i.e. gas darcean permeability) under hydrostatic and deviatoric loading are also under way.

Acknowledgments

The authors are grateful to Th. Dubois, G. Potier (Ecole des Mines de Douai) and M. Davy/P.-A. Coquelin for valuable expertise.

References

[1] R.S. Rostasy, R. Weiss, G. Wiedemann, Changes of pore structure of cement mortar due to temperatures, Cement and Concrete Research 10 (1980) 157–164.
[2] F. Homand, Comportement mécanique des roches en fonction de la température, Editions de la Fondation Scientifique de la Géologie et de ses Applications, 1986.
[3] G.P. Zaraisky, V.N. Balashov, Thermal Decompaction of Rocks in Fluids in the Crust, Chapman & Hall, London, 1994.
[4] D. Gawin, C.E. Majorana, B.A. Schrefler, Numerical analysis of hygro–thermal behaviour and damage of concrete at high temperature, Mechanics of Cohesive-Frictional Materials 4 (1999) 37–74.
[5] L.T. Phan, N.J. Carino, Fire performance of high strength concrete: research needs, in: M. Elgaali (Ed.), Proceedings of the Advanced Technology in Structural Engineering, ASCE/SEI Structures Congress, Philadelphia, 2000.
[6] Y. Xu, Y.L. Wong, C.S. Poon, M. Anson, Influence of PFA on cracking of concrete and cement paste after exposure to high temperatures, Cement and Concrete Research 33 (2003) 2009–2016.
[7] I. Gaweska-Hager, Comportement à haute température des bétons à haute performance - évolution des principales propriétés mécaniques. Thèse de Doctorat (PhD Thesis, in French), Ecole Nationale des Ponts et Chaussées/Ecole Polytechnique de Cracovie, France, 2004.
[8] M. Husem, The effects of high temperature on compressive and flexural strengths of ordinary and high-performance concrete, Fire Safety Journal 41 (2006) 155–163.
[9] Y.F. Fu, Y.L. Wong, C.A. Tang, C.S. Poon, Thermal induced stress and associated cracking in cement–based composite at elevated temperatures–Part II: thermal cracking around multiple inclusions, Cement and Concrete Composites 26 (2004) 113–126.
[10] Y.F. Fu, Y.L. Wong, C.S. Poon, C.A. Tang, P. Lin, Experimental study of micro/macro crack development and stress-strain relations of cement-based composite materials at elevated temperatures, Cement and Concrete Research 34 (2004) 789–797.
[11] F.H. Heukamp, F.-J. Ulm, J.T. Germaine, Poroplastic properties of calcium-leached cement-based materials, Cement and Concrete Research 33 (2003) 1155–1173.
[12] F. Skoczylas, N. Burlion, I. Yurtdas, About drying effects and poro-mechanical behaviour of mortars, Cement Concrete Composites 29 (2007) 383–390.
[13] M.A. Biot, General theory of three—dimensional consolidation, Journal of Applied Physics 12 (1941) 155–164.
[14] O. Coussy, Poromechanics, J. Wiley & Sons, New York, 2004.
[15] R. de Boer, Theoretical poroelasticity - a new approach, Chaos, Solitons and Fractals 25 (2005) 861–878.
[16] V.A. Papathanasopoulou, D.I. Fotiadis, G. Foutsitzi, C.V. Massalas, A poroelastic bone model for internal remodeling, International Journal of Engineering Science 40 (2002) 511–530.
[17] T.H. Smit, J.M. Huyghe, S.C. Cowin, Estimation of the poroelastic parameters of cortical bone, Journal of Biomechanics 35 (2002) 829–835.
[18] D. Fabre, J. Gustkiewicz, Poroelastic properties of limestone and sandstones under hydrostatic conditions, International Journal of Rock Mechanics & Mining Science 34 (1997) 127–134.
[19] D.J. Hart, H.F. Wang, A single test method for determination of poroelastic constants and flow parameters in rocks with low hydraulic conductivities, International Journal of Rock Mechanics & Mining Science 38 (2001) 577–583.
[20] J.R. Rice, M.R. Cleary, Some basic stress-diffusion solutions for fluid-saturated elastic porous media with compressible constituents, Reviews of Geophysics 14 (1976) 227–241.
[21] R.W. Zimmerman, Coupling in poroelasticity and thermoelasticity, International Journal of Rock Mechanics & Mining Science 37 (2000) 79–87.
[22] M. Sibai, L. Dormieux, V. Pensée, D. Kondo, Effets de la microfissuration en poroélasticité des roches: étude expérimentale et analyse théorique, Proceedings of the 16th French Mechanics Congress (CFM), 2003, in French.
[23] M. Lion, F. Skoczylas, B. Ledésert, Determination of the main hydraulic and poro–elastic properties of a limestone from Bourgogne, France, International Journal of Rock Mechanics & Mining Science 41 (2004) 915–925.
[24] M. Lion, F. Skoczylas, B. Ledésert, Effects of heating on the hydraulic and poroelastic properties of Bourgogne limestone, International Journal of Rock Mechanics & Mining Science 42 (2005) 508–520.
[25] F.J. Ulm, G. Constantinides, F.H. Heukamp, Is concrete a poromechanics materials? A multiscale investigation of poroelastic properties, Materials and Structures/Concrete Science and Engineering 37 (2004) 43–58.
[26] J. Sanahuja, L. Dormieux, G. Chanvillard, Modelling elasticity of a hydrating cement paste, Cement Concrete Research 37 (2007) 1427–1439.
[27] R.F. Feldman, P.J. Sereda, A new model for hydrated Portland cement and its practical implications, Engineering Journal (Canada) 53 (8/9) (1970) 53–59.
[28] P.D. Tennis, H.M. Jennings, A model for two types of calcium silicate hydrate in the microstructure of portland cement pastes, Cement and Concrete Research 30 (6) (2000) 855–863.
[29] H.M. Jennings, A model for the microstructure of calcium silicate hydrate in cement paste, Cement and Concrete Research 30 (1) (2000) 101–116.
[30] G. Constantinides, F.J. Ulm, The nanogranular nature of C–S–H, Journal of the Mechanics and Physics of Solids 55 (2007) 64–90.
[31] H.M. Jennings, Refinements to colloid model of C–S-H in cement: CM-II, Cement and Concrete Research 38 (2008) 275–289.
[32] C. Mian, C. Zhida, Effective stress laws for multi-porosity media, Applied Mathematics and Mechanics, English Edition 20 (11) (1999) 1207–1213.
[33] M.D. Bolton, A Guide to Soil Mechanics, Macmillan, London, 1979 (reprinted by Chung Hwa Books, and published by M.D. and K. Bolton in 1991, and 1998).
[34] A. Nur, J.D. Byerlee, An exact effective stress law for elastic deformation of rock with fluids, Journal of Geophysical Research 76 (26) (1971) 6414–6419.

[35] P. Mounanga, Etude expérimentale du comportement de pâtes de ciment au très jeune âge: hydratation, retraits, propriétés thermophysiques. Thèse de doctorat de l'Université de Nantes (PhD Thesis, in French), 2003.
[36] M. Sibaï, Etude de l'interaction fluide squelette dans les roches; méthodes expérimentales et modélisations. PhD thesis, Université des Sciences et Technologies de Lille, France (in French), 1990.
[37] I. Yurtdas, N. Burlion, F. Skoczylas, Experimental characterization of the drying effect on uniaxial mechanical behaviour of mortar, Materials and Structure 37 (267) (2004) 170–176.
[38] I. Yurtdas, N. Burlion, F. Skoczylas, Triaxial mechanical behaviour of mortar: effects of drying, Cement and Concrete Research 34 (2004) 1131–1143.
[39] N. Burlion, D. Bernard, D. Chen, X-ray microtomography: application to microstructure analysis of a cementitious material during leaching process, Cement Concrete Research 36 (2006) 346–357.
[40] I. Yurtdas, H. Peng, N. Burlion, F. Skoczylas, Influences of water-to-cement ratio on mechanical properties of mortars submitted to drying, Cement and Concrete Research 36 (2006) 1286–1293.
[41] F. Skoczylas, Multiphysics processes in concrete, Revue Européenne de Génie Civil, special issue on Multiphysics Geomechanics, vol. 9, 2005, pp. 597–618, (in English).
[42] V. Baroghel-Bouny, Caractérisation microstructurale et hydrique des pâtes de ciment et des bétons ordinaires et à très hautes performances. Thèse de Doctorat (PhD Thesis, in French), Ecole Nationale des Ponts et Chaussées, Paris, 1994.
[43] M. Lion, F. Skoczylas, Z. Lafhaj, M. Sersar, Experimental study on a mortar. temperature effects on porosity and permeability. Residual properties or direct measurements under temperature, Cement and Concrete Research 35 (2005) 1937–1942.
[44] H. Colina, P. Acker, Drying cracks: kinematics and scale laws, Materials and Structure 33 (2000) 101–107.
[45] M.C.R. Farage, J. Sercombe, C. Gallé, Rehydration and microstructure of cement paste after heating at temperatures up to 300 °C, Cement and Concrete Research 33 (2003) 1047–1056.
[46] A.M. Neville, Properties of Concrete, 4th Ed. Wiley & Sons, 1996.
[47] J. Xiao, H. Falkner, On residual strength of high-performance concrete with and without polypropylene fibres at elevated temperatures, Fire Safety Journal 41 (2006) 115–121.
[48] C.A. Davy, M.D. Bolton, N.A. Fleck, The shearing behaviour of a sugar aggregate, Acta Materialia 52 (2004) 3587–3601.
[49] R. Kherbouche, Etude du comportement poro-élasto-plastique de la craie. Thèse de Doctorat (PhD Thesis, in French), Université des Sciences et Technologies de Lille, France, 1994.
[50] G.F. Peng, Evaluation of fire damage to high performance concrete. PhD thesis, The Hong Kong Polytechnic University, Hong Kong, 1999.
[51] C.R. Cruz, M. Gillen, Thermal expansions of Portland cement paste, mortar and concrete at high temperature, Fire and Materials 4 (1980) 66–70.
[52] N. Hearn, Effect of shrinkage and load-induced cracking on water permeability of concrete, ACI Materials Journal 96 (2) (1999) 234–241.
[53] J. Bisschop, J.G.M. van Mier, How to study drying shrinkage microcracking in cement–based materials using optical and scanning electron microscopy, Cement Concrete Research 32 (2002) 279–287.
[54] Z.P. Bažant, M.F. Kaplan, Concrete at High Temperatures: Material Properties and Mathematical Models, Longman Group, England, 1996.
[55] A. Noumowé, Effet des hautes températures (20-600 °C) sur les bétons, cas particulier du béton à hautes performances. Thèse de doctorat (PhD Thesis, in French), 1995.
[56] A. Loukili, A. Khelidj, P. Richard, Hydration kinetics, change of relative humidity, and autogenous shrinkage of ultra-high-strength concrete, Cement and Concrete Research 29 (1999) 577–584.
[57] A.H.-D. Cheng, Y. Abousleiman, Intrinsic poroelasticity constants and a semi—linear model, International Journal for Numerical and Analytical Methods in Geomechanics 32 (2008) 803–831.
[58] F. Homand, J.F. Shao, A. Giraud, C. Auvray, D. Hoxha, Pétrofabrique et propriétés mécaniques des argilites, Comptes Rendus – Geoscience 338 (12-13) (2006) 882–891.